ASIA-PACIFIC JOURNAL OF ATMOSPHERIC SCIENCES, 45, 1, 2009, p. 55-69

An Application of Brightness Temperature Received from a Ground-based Microwave Radiometer to Estimation of Precipitation Occurrences and Rainfall Intensity

Hye Young Won, Yeon-Hee Kim, and Hee-Sang Lee

Forecast Research Laboratory, National Institute of Meteorological Research, KMA

(Manuscript received 19 September 2008; in final form 20 January 2009)

Abstract

Ground-based microwave radiometers (MWR) provide continuous thermodynamic (temperature, water vapor, and cloud liquid) soundings in the clear and cloudy weather conditions. These profiles can be determined by observing the intensity of the atmospheric radiation at selected frequencies. The MWR used in this study is TP/WVP-3000A, which measures the intensity of radiation at 8 water vapor channels (22-30 GHz) and 14 oxygen channels (51-59 GHz) to obtain thermodynamic profiles at National Center for Intensive Observation of severe weather (NCIO) located at Haenam, Korea. In this study, the predictability of precipitation occurrences and the estimation of rainfall intensity were investigated by using the brightness temperature (TB) of the MWR. The averaged differences of TBs in 2 hours before raining were calculated and compared with those of period unrelated with rain. In 2 hours before raining, the pronounced increase of TB was observed in water vapor channels (22-30 GHz), while TBs in 54-59 GHz as oxygen channels were almost remaining constant except for the great increase of TB at 51-52 GHz related to cloud liquid water. Performance for forecasts of precipitation occurrences using the preceding increases of TBs at 22.2 GHz, 30.0 GHz, and 51.2 GHz was improved and better than the 3-hour operational (routine) forecasts. The estimation of rainfall intensity was examined by two simple estimative methods using the linear and the nonlinear regression analyses between rainfall intensity and TBs. Rainfall intensity was estimated by the calculated regression curves of TBs from MWR and compared with observed one by an Optical Rain Gauge (ORG) at the Haenam NCIO. As a result of the verification on forecasting performances, both the linear and the logarithmic regression methods between the observed and the estimated rainfall intensity showed substantially high in Equitable Threat Scores (ETSs) and correlation coefficients.

Key words: Microwave radiometer (MWR), brightness temperature (TB), precipitation occurrences, rainfall intensity, KEOP

1. Introduction

A correct forecast of precipitation occurrences and the rainfall amount is demanded because rainfall information is important in various fields such as agriculture and water resource management as well as a weather forecast. More detailed information about the thermodynamic structure of the atmosphere (up to 10 km height) is required for the specific precipitation forecast. Ordinary upper-air observation performed by a radiosonde only 2 times (0000, 1200 UTC) a day is not sufficient to monitor atmospheric structures vertically for a short-term forecast because precipitation systems develop rapidly (Güldner and Spänkuch, 1999).

To observe continuously the atmosphere in the boundary layers for various reasons, for example, a short-term weather forecast and air pollution control, many previous studies have used various remote sensing instruments such as the wind profiler, radar, lidar, and MWR even if it is common knowledge that they have uncertainty (Clifford *et al*., 1994; Güldner and Spänkuch, 2001; Wilczak *et al*., 1996). Specially, the MWR in the advantage of continuous monitoring has been widely and successfully operated to cover the temporal and spatial gaps of synoptic

Corresponding Author: Yeon-Hee Kim, Forecast Research Laboratory, National Institute of Meteorological Research, KMA, 45 Gisangcheong-gil, Dongjak-gu, Seoul, 156-720, Korea.
Phone : +82-2-6712-0253, Fax : +82-2-834-5922
E-mail: kyh@kma.go.kr

networks by radiosonde measurements. The MWR is also less restrictive in observation than the geostationary satellite which cannot scan the same regions continuously as the rotation of the earth. Guiraud *et al.* (1979) also indicated that ground-based microwave radiometer data can be used to monitor precipitable water vapor (PWV) better than conventional radiosonde data.

Developed countries and universities in numerical forecast fields, for example, University of Oklahoma, USA and McGill University, Canada, have carried out various experiments with the radiometric soundings in numerical weather forecast and severe weather nowcasting. Ware *et al*. (2003) compared radiometric profiles with radiosonde and forecast sounding in the evaluation of the accuracy of radiometric temperature and water vapor soundings and further described a case study which showed the improved fog forecasting on the basis of variational assimilation of radiometric soundings. Chan and Tam (2005) presented the performance and application of an instability index (K-index) derived from the MWR for the nowcasting of heavy rainfall and thunderstorms during a field experiment conducted in Hong Kong. Several studies have also been made to analyze the continuous profiles and physical variables retrieved from the MWR. For examples, Barbaliscia *et al.* (1998) discussed the cumulative distributions of the TB as well as those of the integrated water vapor (IWV) and the liquid water content (LWC) retrieved via the radiometric measurements for 4 years in Italy. The analysis was performed for various time bases: years, months, and hours of the day. Doran *et al.* (2002) also examined the differences in cloud liquid water path (LWP) at a coastal and an inland location on the north slope of Alaska using the MWR data.

The PWV retrieved from the MWR measurements in Daegwallyeong has been compared with that of Global Positioning System (GPS) (Ha *et al.*, 2007) and that of radiosonde measurements (Chang *et al.*, 2007). Yang *et al.* (2006) validated PWV from the MWR by comparing with that of radiosonde observed during 2001-2003 and presented the seasonal biases of PWV between the MWR and radiosonde measurements.

Güldner and Spänkuch (1999) showed increases in parameter of LWC and PWV in 2 hours before raining. These findings encouraged us that there is an ample hope for short-term local precipitation forecast by using the MWR. Also, Liu *et al*. (2001) used the radiometry data to establish an algorithm for the estimation of the rainfall intensity and to find the optimal time period for comparing with rain gauge data.

In this study, the predictability of precipitation occurrences and the estimation of rainfall intensity using the TBs from the MWR in the NCIO located at Haenam (34.55°N, 126.57°E), Korea are investigated and the performances and applications of the MWR as a tool for short-term precipitation forecasts are discussed.

This paper is organized as follows: the overview and specification of a ground-based microwave radiometer is described in section 2. The methods, results and verification for the predictability of precipitation occurrences and the estimation of rainfall intensity are presented in section 3 and section 4, respectively. Summary of this study is presented in section 5.

2. Ground-based Microwave Radiometer

The Automatic Weather System (AWS), Automatic Balloon Launcher (ABL or Autosonde), Wind profiler (WPR), ORG, and Micro Rain Radar (MRR) for the ordinary and intensive observation in the Haenam NCIO are being operated by National Institute of Meteorological Research (NIMR) (Meterological Research Institute, 2003, 2004, 2005, 2006). The MWR (TP/WVP-3000A) has been installed in the Haenam NCIO on 22 August 2007 and is being operated to provide the profiles of temperature, relative humidity, water vapor, and liquid water in real-time as a key instrument of the high-impact weather observing system for severe weathers.

The MWR measurements are mainly available in the clear and cloudy but not in the rainy weather conditions because water beads on the outer housing (radome) make less accurate in radiometric measurements. Recently, however, there are some prog-

ress in applying rain-effect mitigation methods to the MWR such as a hydrophobic radome and forced airflow over the radome surface. An equipment named the 'superblower' is mounted in the MWR at the Haenam NCIO and is used to sweep water beads and snow away from the rain sensor which is mounted on the top of the blower system. The ambient temperature and relative humidity sensors are integrated in the inlet of the blower system to ensure a steady flow of ambient air over the sensors, which is commensurate with Chan and Tam (2005) result that MWR shows good performances in the subtropical heavy rainfall (30 mm h^{-1}). Further details of performance of the MWR at the Haenam NCIO in rainy weather conditions are shown in Jeon *et al*. (2008).

In short, the instrument specification and the operational theory of the MWR of the Haenam NCIO are presented in Table 1 and Fig. 1, respectively. It measures the intensity of the atmospheric radiation at 8 water vapor channels (K-band) and 14 oxygen channels (V-band) along with zenith infrared, and then the TBs (Level 1 data) are converted via Planck's Law. Historical radiosondes and neural network methods are used for profile retrieval (Level2 data). The surface meteorological measurements (temperature, relative humidity, pressure) and infrared thermometer (IRT) measurements are also required for determination of temperature, water vapor, and liquid water profiles (Fig. 1a) (National Institute of Meteorological Research, 2007).

Table 1. Instrument specification.

Function or Parameter	Specification
Frequencies	
	22 - 30 GHz
water vapor band	22.2, 22.5, 23.0, 23.8, 25.0, 26.2, 28.0, 30.0,
	51 - 59 GHz
oxygen band	51.2, 51.7, 52.2, 52.8, 53.3, 53.8, 54.4, 54.9, 55.5, 56.0, 56.6, 57.2, 57.9, 58.8
minimum frequency step size	4.0 MHz
Pre-detection channel bandwidth	300 MHz
Antenna system optical resolution and side lobes	
22-30 GHz	4.9 - 6.3° -24dB
51-59 GHz	2.4 - 2.5° -27dB
Integration time	0.01 to 2.5 seconds
Physical properties	
size (H × W × L)	50 × 28 × 76 cm
weight	29 kg

The microwave profiling methods make use of atmospheric radiation measurements from 20 to 60 GHz region. The zenith path atmospheric absorption spectrum at sea level for a typical mid-latitude atmosphere with a 1 km thick, 0.5 g m^{-3} cloud in the frequency band is shown in Fig. 1(b). Two altitudes and two water vapor densities are shown as well as radiometer tuning bands, marked by bold lines. The feature at 22.2 GHz is a water vapor resonance that is pressure broadened according to the pressure altitude of the water vapor distribution, while the feature at 60 GHz is an atmospheric oxygen resonance. The cloud liquid water spectrum increases approximately with the second power of frequency in this region. Then, temperature profiles can be obtained by measuring the spectrum of radiation intensity or TB at points along the side of the oxygen feature at 60 GHz, water vapor profiles by observing the intensity and shape of emission from pressure broadened water vapor lines, and cloud liquid water profiles by combining 22 to 30 GHz and 51 to 59 GHz turning bands utilized by the MWR at the Haenam NCIO (Solheim *et al*., 1998).

The MWR at the Haenam NCIO uses the neural networks method to determine thermodynamic profiles because neural networks outperform other methods for retrievals (Solheim *et al.*, 1998; Radiometrics Corp., 2007). Meanwhile, Kim and Baik (2002) proved that the neural network model improves upon the regression model. The reason for the improvement of the neural network model upon the multiple linear regression model is that the neural network has an internal ability to take complex nonlinear interaction into account. This ability is achieved by including the nonlinear activation function in the neural network. The above results indicate that it might be possible to develop a multiple nonlinear regression model that competes with a neural network model if a nonlinear functional relationship is well chosen. The neural networks are derived using the

(a)

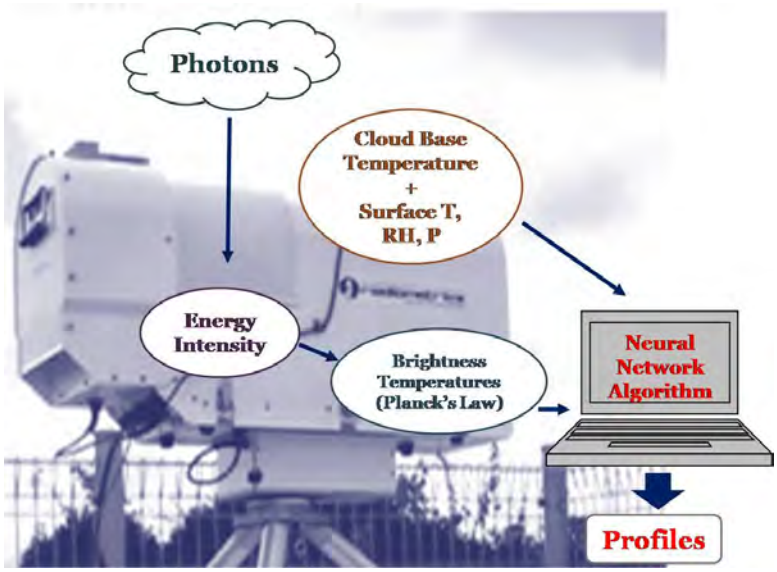

(b)

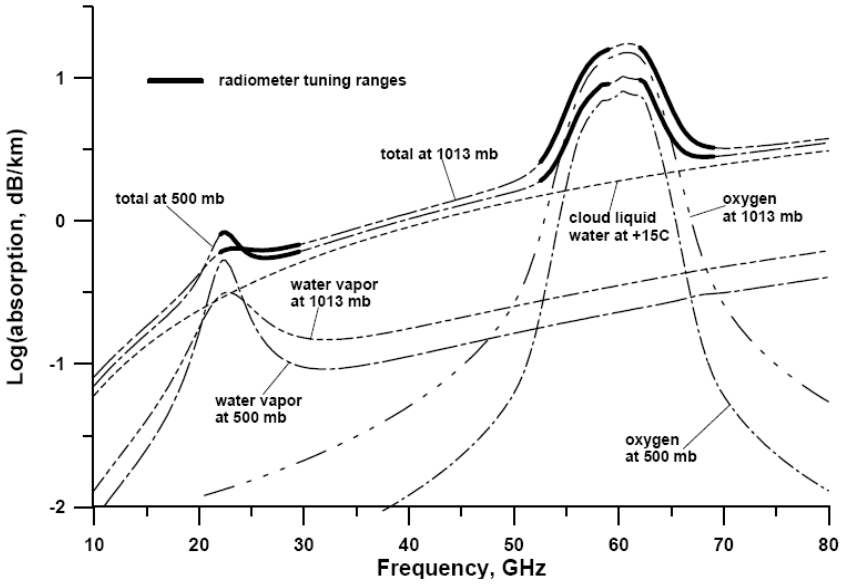

Fig. 1. (a) The receiving/processing data procedure of the MWR (Radiometrics TP/WVP-3000A) at the Haeanm NCIO and (b) the vertical distribution of atmospheric absorption spectrum [from Solheim *et al*. (1998)].

Stuttgart Neural Network Simulator (SNNS) and a history of radiosonde profiles. A standard back-propagation algorithm is used for training and a standard feed-forward network is used for profile determination. Five-year radiosonde data at Gwangju site (35.11°N, 126.81°E) in the same climatological region were used as the historical radiosonde soundings. Above approximately 7 km, atmospheric water vapor density and temperature approach to the climatological mean values. Profiles are set to a total of 58 levels up to 10.0 km: precisely, 50 m levels from the surface to 0.5 km, 100 m levels from 0.5 km to

2.0 km, and 250 m levels from 2.0 km to 10.0 km.

Because PWV and LWC profiles (Level 2) are retrieved from TBs data (Level 1) using historical radiosondes and neural network methods, TBs as a primitive parameter would be more accurate than PWV and LWC. Therefore, TBs data are used in this study instead of the retrieved profiles such as PWV and LWC.

3. Predictability of precipitation occurrences and its verification

To investigate the predictability of precipitation occurrences, first, *Rain Events* were selected using 15-minute moving-accumulated rainfall data by AWS (15-min AWS rainfall data) at the Haenam NCIO. If a *Rain Event* reoccurred in the interval of 2 hours after the termination of the previous *Rain Event*, it was regarded the same as the previous *Rain Event*. When the time interval of TB difference is chosen to be shorter than 2 hours, preceding time to predict the precipitation occurrences could not be ensured. If the larger time intervals than 2 hour (3, 6, 12, 24, etc.) were considered, only a few number of *Rain Events* were included in this study. So, the 2-hour interval is used in this study as in other literature (Güldner and Spänkuch, 1999).

Now, two datasets, **RR** (Rain Record) and **NR** (No-rain Record), were created to examine the changes of TBs before raining. **RR** is comprised of TBs data from MWR in the interval of 2 hours before each *Rain Event*. To eliminate seasonal dependence and weekly cycle of both data sets (**RR** and **NR**), **NR** data set was selected at the same time in corresponding time period of 7 days later. Then TBs data were excluded from **NR** if it rained during the 2-hour interval, which makes **NR** be no related with rain (Fig. 2). As a result, the sample number is as many as 102 and 91 respectively from 23 August 2007 to 30 June 2008 (about 10 months).

Fig. 3 shows the accumulated rainfall amount of each *Rain Event*. The accumulated rainfall amount

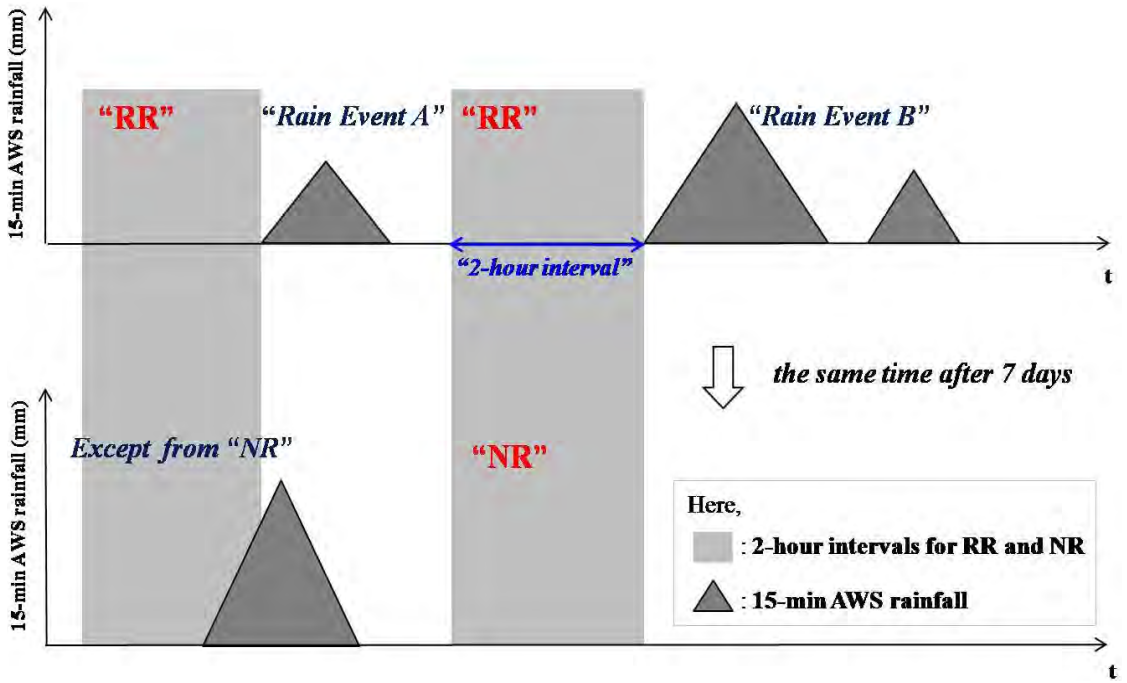

Fig. 2. A brief diagram for the definition of the *Rain Events*, **RR** (Rain Record), and **NR** (No-rain Record) data set. The shaded triangles and boxes mean 15-min AWS rainfall (mm) and 2-hour intervals for **RR** and **NR**, respectively. **RR** is comprised of TBs data in 2-hour interval before raining and **NR** is at the same time after 7 days except for raining.

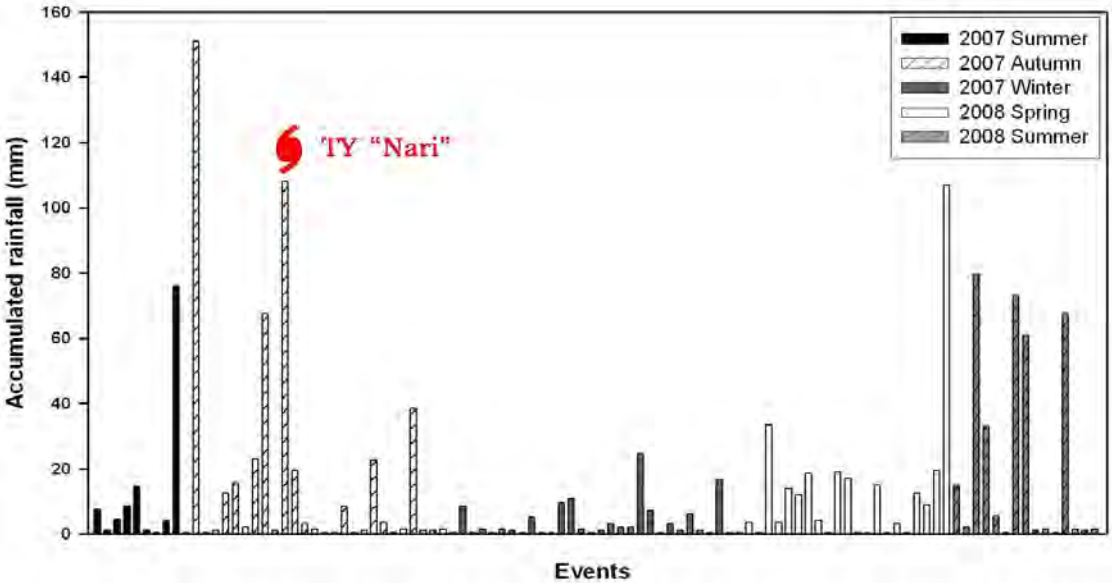

Fig. 3. Accumulated rainfall amount of each *Rain Event* during the period from 23 August 2007 to June 30 2008. The vertical bars mean the accumulated rainfall of each *Rain Event* and are distinguished into each season. A heavy rainfall event is marked by typhoon symbol ( ).

in autumn, 2007 is greater than that in summer. For the accumulated rainfall amount per a *Rain Event*, however, it is revealed that the accumulated rainfall amount per a *Rain Event* is larger in summer (15 mm per event)) than in autumn (5 mm per event) even if heavy rainfall event by a typhoon "NARI" also occurred in fall, 2007. It generally rained a little in winter and there are two snowfall events (not shown).

The differences of TBs between 2-hour before raining (*-2 h*) and each time (t, $-2.0\ h \leq t < 0.0\ h$) in **RR** and **NR** are calculated, respectively and the averaged differences of **RR** and **NR** at 10 channels are presented in Fig. 4. In **RR** concerned with *Rain Events*, the averaged difference gradually increases and the remarkable jump in 30 minutes before raining (-0.5 hour before raining) is shown while there is no difference of TB in **NR** (unrelated with rain). These results are similar to the substantial increase of regression lines of PWV and LWC deviations from 2-hour mean in the last 30-minute subinterval shown by Güldner and Spänkuch (1999). In comparison with the averaged differences of TB according to each frequency, the great increases are observed before raining at water vapor band (22-30 GHz) while the averaged differences of TBs from 54 to 59 GHz in V-band channels are almost remaining except for the prominent increases at 51-52 GHz related to cloud liquid water. These results imply that the channels from 54 to 59 GHz are not suited for the forecasts of precipitation occurrences. When the same method calculating the differences of TBs before raining was applied to PWV and LWC, the averaged differences of PWV and LWC similarly appeared before raining. But they are not enough for the forecasts of precipitation occurrences in comparison with those of TBs (not shown).

The mean and standard deviation of TBs in *Rain Events* and *No Rain Events* (hereafter, by defining when 0.0 mm rainfall is detected from 15-min AWS rainfall data) were also calculated to discuss the characteristics of TB distributions (Fig. 5). From 54 to 59 GHz, the differences in the mean value of TBs between *Rain Events* and *No Rain Events* are only a little about 6.5 K and standard deviations are smaller than mean values of TBs. It means that the unchanged TBs

(a) **RR**

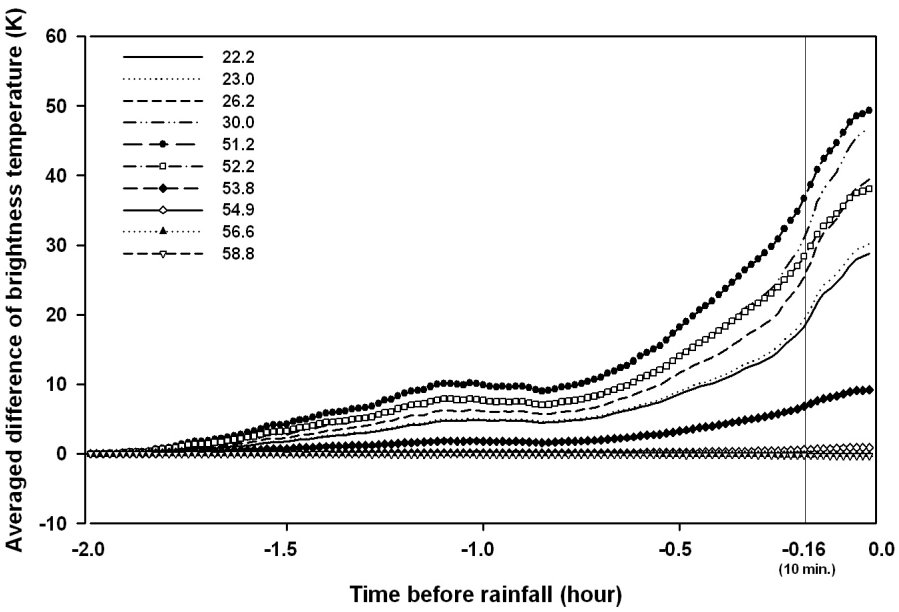

(b) **NR**

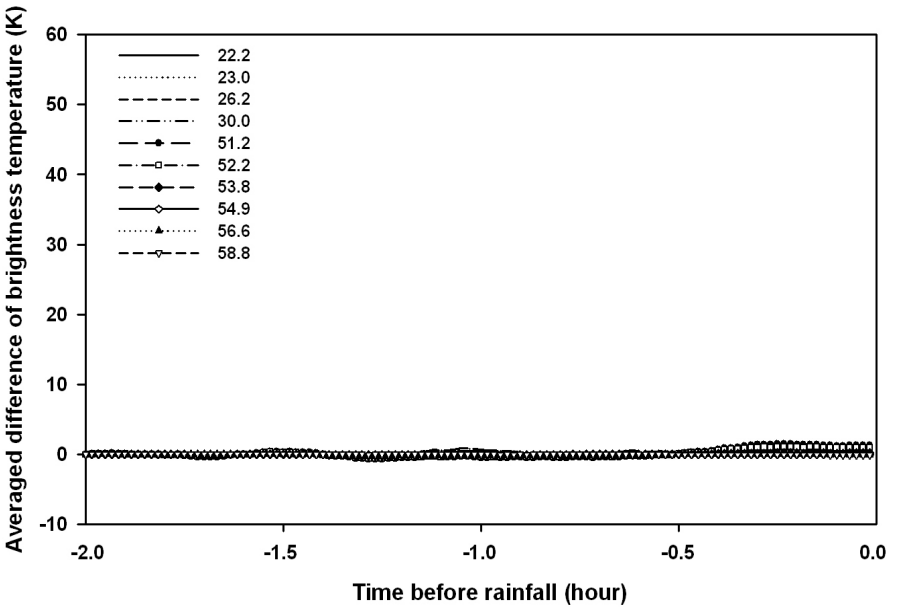

Fig. 4. The averaged differences of TB between 2-hour (*-2 h*) before raining and each time (*t*) at each frequency for (a) 102 records in **RR** and (b) 91 records in **NR**, respectively. The x-axis of each chart means the time before precipitation occurrences.

at these frequencies are unrelated to precipitation phenomena. The differences in the mean value of TBs between *Rain Events* and *No Rain Events* at 22-30 GHz are more or less large and the standard deviations are mainly large. That means that TBs at the V-band are widely distributed. Frequencies in 30.0 GHz and 51.2 GHz have the greatest differences in the mean value of TBs between *Rain Events* and *No*

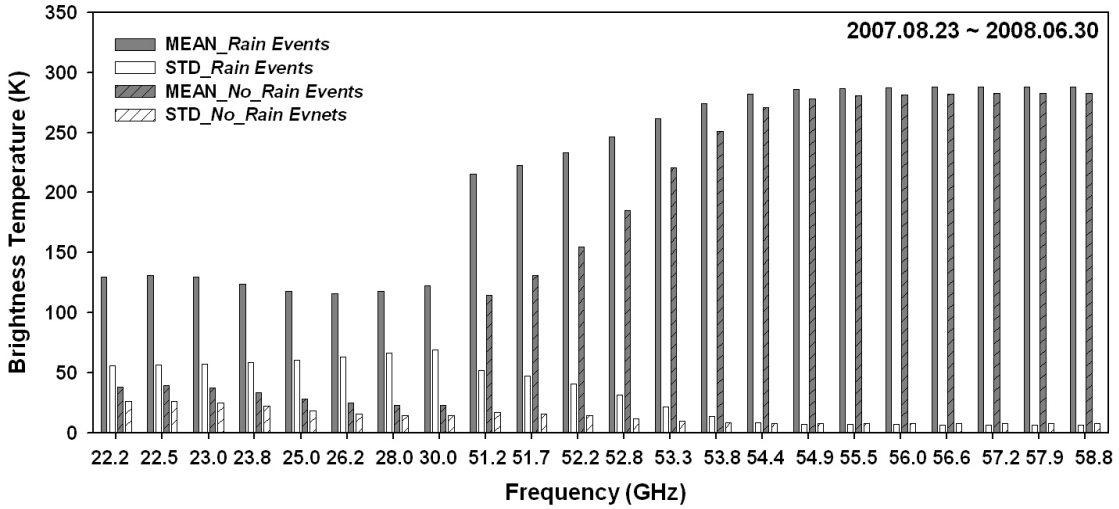

Fig. 5. The mean and standard deviation of theTBs at each frequency of *Rain Events* (filled bars) and No *Rain Events* (lined bars). The gray and white bars represent statistical value (mean and standard deviation) of *Rain Events* and *No Rain Events*, respectively.

Rain Events at the K-band and V-band, respectively, which are the same channels showing the large differences of TBs before raining.

Based on the averaged differences of TBs before raining and the distributions of TBs (Figs. 4 and 5), three channels are selected to predict precipitation occurrences. Two channels, 30.0 GHz and 51.2 GHz, showing the biggest averaged differences of TB before raining and the largest differences in the mean value of TBs between *Rain Events* and *No Rain Events* are selected as factors for the forecasts of precipitation occurrences. Frequency 22.2 GHz is also used as a factor since this frequency shows the least value in the averaged difference of TBs before raining in the whole K-band. These three channels should ensure the maximum and minimum differences of TBs before raining, and therefore they are used as factors to predict precipitation occurrences. The lagged correlation between the differences of TBs and rainfall amount in each *Rain Event* is calculated to examine when the rainfall phenomena are mostly concerned with the differences of TBs before raining, and then to determine thresholds in differences of TBs. Fig. 6 shows that the lagged correlation coefficients at three channels gradually increase in 2 hours and the abrupt increases appear in 30 minutes before raining, which shows the same results with the averaged difference of TBs (Fig. 4a). Lagged correlation coefficients reach to their peaks at the last 10-minute before raining, which are 0.62, 0.67, and 0.75 at 22.2 GHz, 30.0 GHz and 51.2 GHz, respectively. Based on this statistical analysis, the differences of TBs at the last 10-minute before raining are used as thresholds for the forecasts of precipitation occurrences. Threshold values are 18 K, 30 K, and 35 K at 22.2 GHz, 30.0 GHz, and 51.2 GHz, respectively.

Also, variations of TBs are defined as the differences of TBs between before 2-hour and every minute and calculated at three channels in whole period from 23 August 2007 to 30 June 2008. Some examples of the variation of TBs are presented in Fig. 7. According to the rain contingency table (Wilks, 1995) consisting of dichotomous forecasts, "yes" and "no", about occurrences of any phenomena (Table 2), "Hit" indicates that the precipitation is observed by AWS when precipitation occurrence is predicted, and "Miss" does when not predicted. "False Alarm" represents that precipitation occurrence is predicted when the precipitation is not occurred (Fig. 7).

From 23 August 2007 to 30 June 2008, forecasts of precipitation occurrences were performed by using the variations of TBs and evaluated by the several

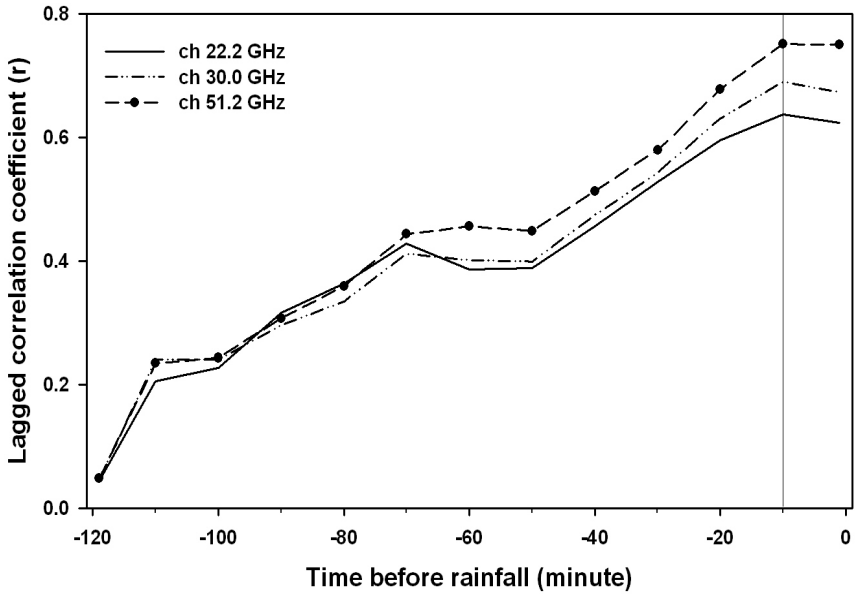

Fig. 6. The lagged correlation coefficient (r) between the differences of TBs in 2-hour interval before raining and rainfall amount in each *Rain Event* at three channels. The vertical line indicates the last 10-minute before raining.

Table 2. Rain contingency table.

		Forecast	
		Yes	No
Observation	Yes	**H (hits)**	**M (misses)**
	No	**F (false alarms)**	**Z (zero)**

verification indices, which are summarized in Table 3. Fig. 8 shows the performance of MWR in comparison with that of 3-hour operational forecasts which mean the 3-hour interval operational forecasts of precipitation occurrences during next 3 hours. To eliminate the difference of forecast time interval between MWR and 3-hour operational forecasts capacity, the 3-hour interval MWR related forecast and the operational forecast issued at Wando observatory (34.40°N, 126.70°E) are compared during the period from August 2007 to June 2008 and shown in Fig. 8a. Judging from smaller BIS, FAR and larger CSI by using TBs from the MWR, the MWR is capable of having better performance than 3-hour operational forecasts. While the POD by the MWR is rather smaller than that by operational forecasts, the POD according to the accumulated rainfall amount is calculated (Fig. 8b). When the accumulated rainfall is less than 3.0 mm, the POD is less than 0.4. This result supports that forecasts by the MWR are unavailable for light rainfall (less than 0.3 mm). However, the POD of the *Rain Events* more than 3.0 mm almost reaches over 0.8. The performance of the MWR indicates that there is the predictability of the precipitation occurrences using the variations of TB from the MWR.

4. Estimation of rainfall intensity and its verification

Two estimation methods for the rainfall intensity are examined by a good relationship between the rainfall intensity and TBs from a MWR (Liu *et al.*, 2001). This study is not focused on which method is better, but an application of two methods to the MWR at the Haenam NCIO and its performances.

The first method (RIE1) determines the relationship between 1-hour changes in rainfall intensity and TBs because the TBs in microwave frequency are influenced by the precipitation. RIE1 can be written as follows:

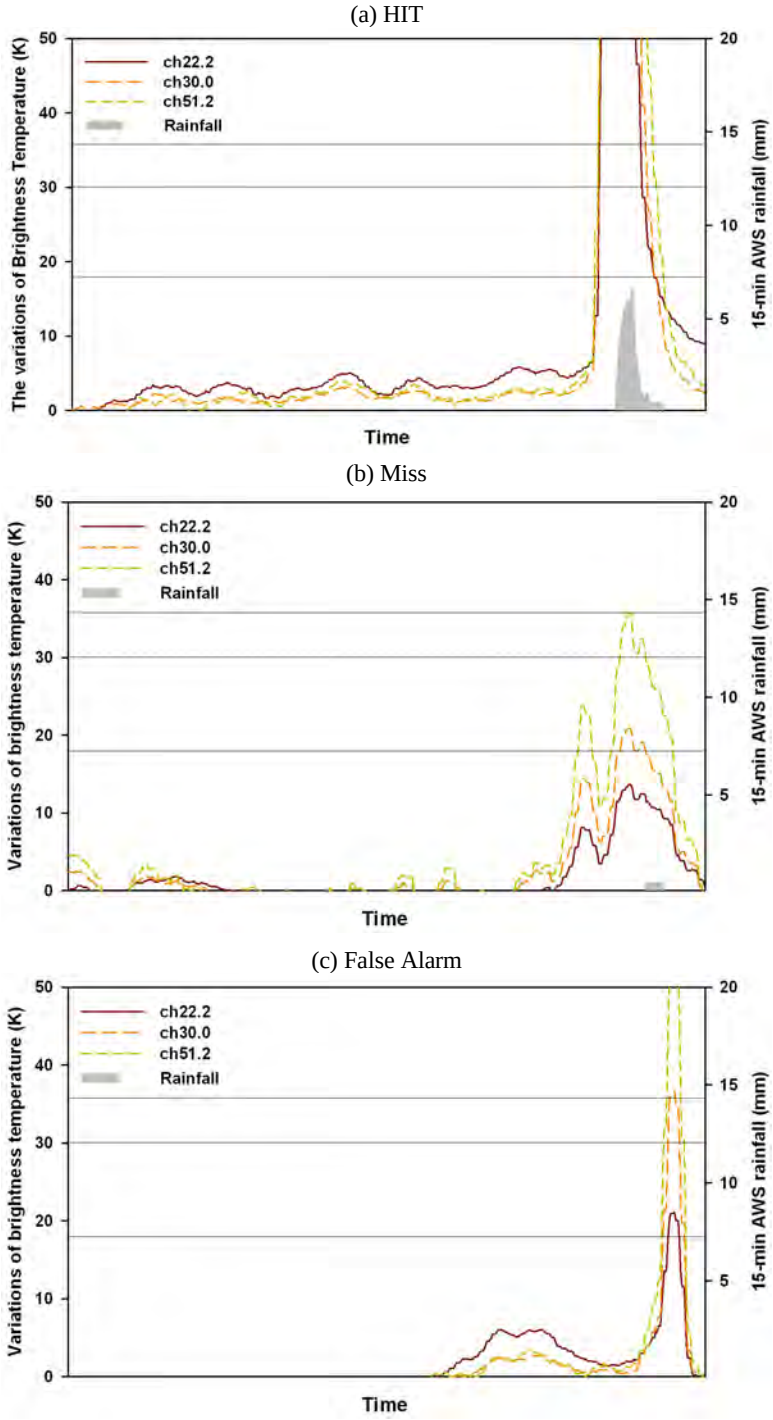

Fig. 7. A brief diagram for forecasts of precipitation occurrences with the variation of TBs. (a) Hit indicates that the precipitation is observed by AWS precipitation occurrence is predicted. (b) Miss indicates that the precipitation is observed by AWS when precipitation occurrence is not predicted. (c) False Alarm represents that precipitation occurrence is predicted when the precipitation is not occurred.

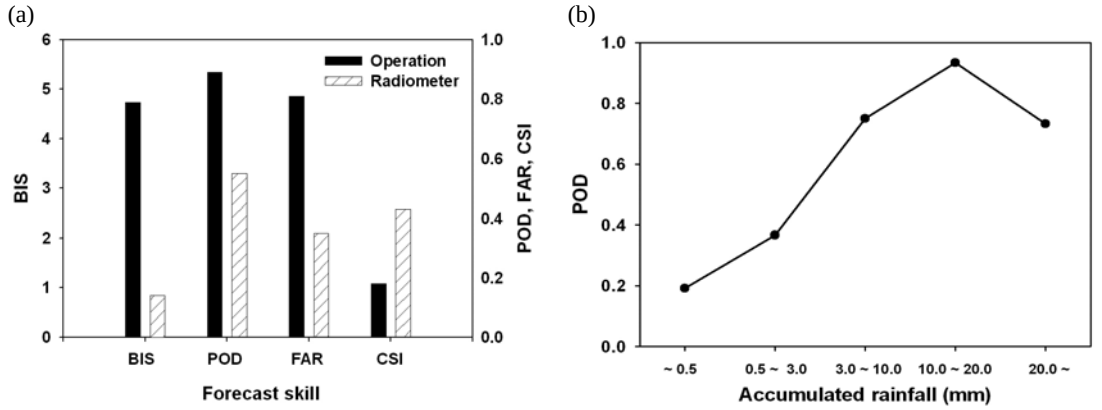

Fig. 8. (a) Qualitative analysis of the rainfall using the some indices (refer to Table 3) and (b) POD (Probability of Detection) according to the accumulated rainfall of each *Rain Event*. Black vertical bars and white-slashed bars mean the forecast skills by the 3-hour operational forecast issued at Wando observatory and by the MWR at the Haenam NCIO, respectively.

Table 3. Summary of some indices for qualitative analysis of the rainfall.

Index	Meaning	Range	Equation
BIS (Bias Score)	How did the forecast frequency of "yes" events compare to the observed frequency of "yes" events?	0 ~ ∞	$BIS = \frac{F+H}{H+M}$
POD (Probability of Detection)	What fraction of the observed "yes" events were correctly forecast?	0 ~ 1	$POD = \frac{H}{M+H}$
FAR (False Alarm Ratio)	What fraction of the predicted "yes" events actually did not occur?	0 ~ 1	$FAR = \frac{F}{F+H}$
CSI (Critical Success Index)	How will did the forecast "yes" events correspond to the observed "yes" events?	0 ~ 1	$CSI = \frac{H}{H+M+F}$
ETS (Equitable Threat Score)	The CSI adjusted for correct forecasts due to random chance.	-1/3 ~ 1	$ETS = \frac{H-R}{H+M+F-R}$ $R = \frac{(M+H)(F+H)}{H+M+F+Z}$

H : Hit **M** : Miss **F** : False Alarm **Z** : Zero **R** : Random hit

$$R_i = R_{i-1} + \triangle R_i \quad (1)$$

$$\triangle R_i = a + b \triangle TB_i \quad (2)$$

where, R and i are the rainfall intensity and the time index, respectively. a and b in Eq. (2) are the curve-fitting coefficients. The 1-hour change in the rainfall intensity can be derived easily by substituting 1-hour change in the TB. The second one (RIE2) uses the relationship between the TB and the instantaneous rainfall intensity as follows:

$$R = a + b \ln(280 - TB) \quad (3)$$

The rainfall intensity can be derived by substituting the observed TB into Eq. (3). The TBs at 30.0 GHz which changed greatly before raining in water vapor band are applied into Eqs. (1), (2), and (3).

ORGs are not affected by any environmental factors which cause significant error with traditional rain and snow gauges and make observations of the rainfall intensity and the accumulated rainfall with high resolution in time. The instrument of ORG at the Haenam NCIO has higher resolution (0.001 mm) for the measurement of rain amount than that of tipping-bucket gauge (conventional rain gauge) at the Haenam NCIO and also measures rainfall intensity

with high time resolution (10 seconds). That is the reason that rainfall intensity data from ORG are used in this study. On the basis of the previous studies (Chan and Tam, 2005), only the rainfall intensity data more than 0.3 and less than 30.0 mm h^{-1} are analyzed, though the superblower is attached to the MWR at the Haenam NCIO. A half of 10-month MWR and ORG data (23 August 2007 - 31 January 2008) are taken as training data to determine the curve-fitting lines for the coefficients in Eqs. (2) and (3) and the another

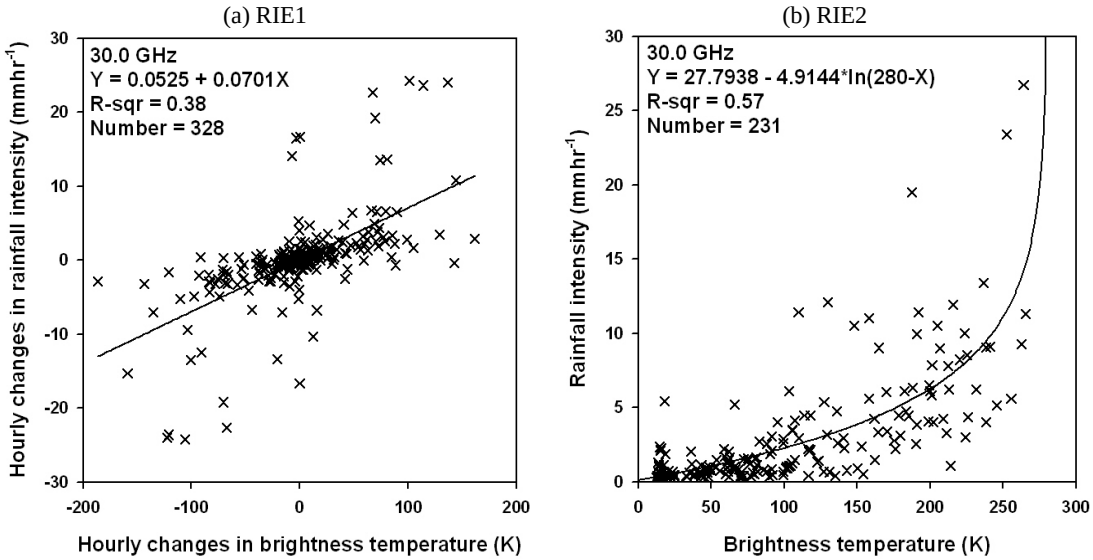

Fig. 9. (a) The relationship between hourly changes in TB at 30.0 GHz and rainfall intensity using the RIE1 method. (b) is the same as (a) but for between TB and rainfall intensity using the RIE2 method. The sample number of the RIE1 and RIE2 is 328 and 231, respectively.

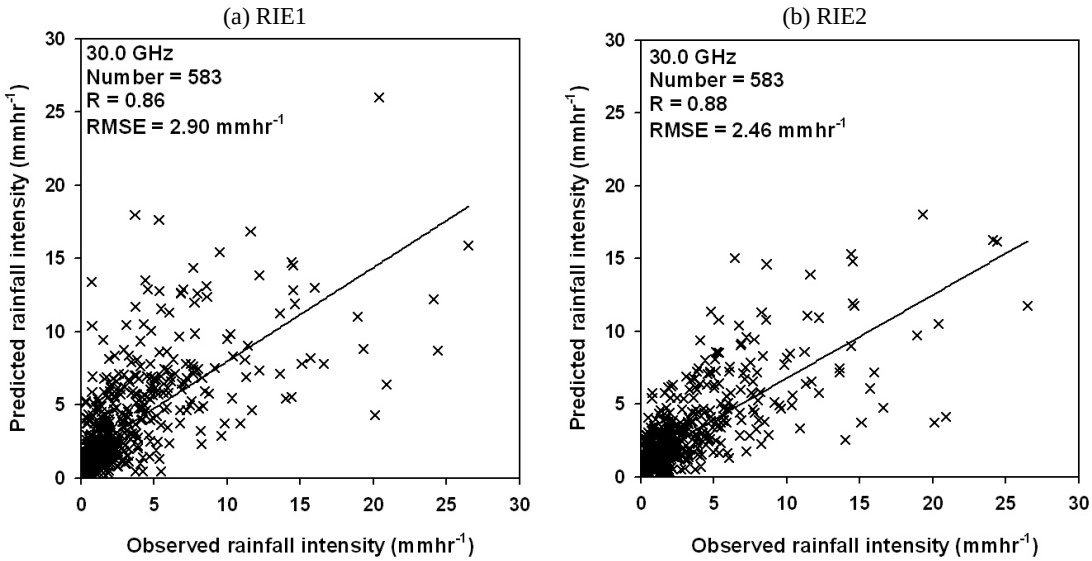

Fig. 10. The relationship between the observed rainfall intensity and predicted rainfall intensity by the (a) RIE1 method and (b) RIE2 method.

half of them (1 February 2008 - 30 June 2008) remained to be used for the verifications.

Regression analysis results between the rainfall intensity from ORG and TBs from the MWR by RIE1 and RIE2 are shown in Fig. 9. Coefficients of determination (R^2) in RIE1 and RIE2 are 0.38 and 0.57, respectively. For RIE1 case, R^2 is smaller than that of RIE2 because the 1-hour changes in rainfall intensity could not catch up large 1-hour changes in TBs (±100.0 K). It seems that these errors may bring overestimation or underestimation of the rainfall intensity. In virtue of two deduced curve-fitting lines shown in Fig. 9, the forecast of the rainfall intensity is performed and the relationship between the observed rainfall intensity by ORG and predicted one by TBs from the MWR is calculated and presented in Fig. 10. The correlation coefficient is 0.86 in RIE1 and 0.88 in RIE2 and root mean square error (RMSE) is 2.90 mm h^{-1} and 2.46 mm h^{-1}, respectively. Several verification indices (refer to Table 3) for the rainfall intensity are also calculated and their performances are presented in Fig. 11. The threshold values get smaller, the POD and ETS get larger, and FAR becomes smaller while BIS gets closer to 1. As a result, it is considered that both RIE1 and RIE2 are available methods for the successful and accurate forecasts of the rainfall intensity, moreover RIE2 method is better than RIE1.

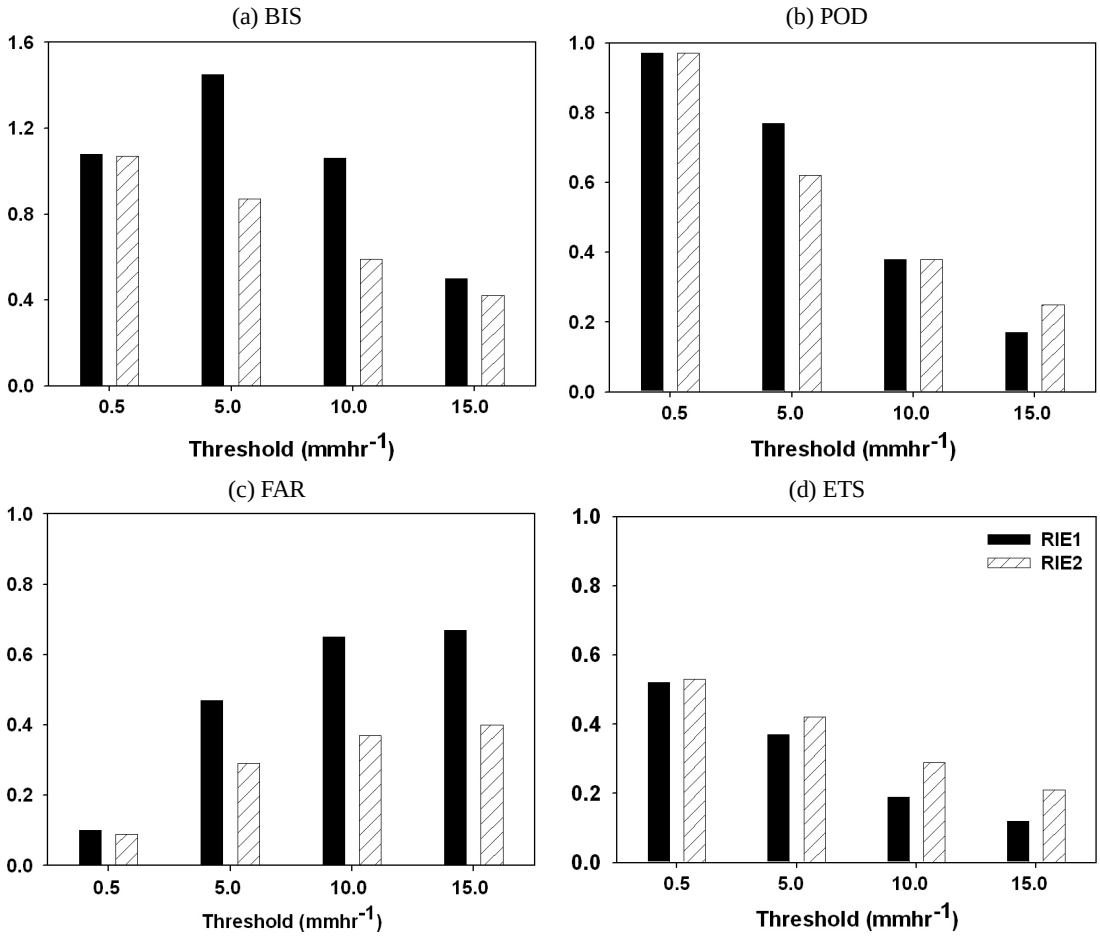

Fig. 11.(a) Bias Score (BIS), (b) Probability of Detection (POD), (c) False Alarm Ratio (FAR), and (d) Equitable Threat Score (ETS) at each threshold value by the RIE1 method (black bars) and RIE2 method (white-slashed bars).

5. Summary

The MWR has being operated at the Haenam NCIO since 22 August 2007 and provided the continuous profilers (e.g., temperature, relative humidity, water vapor, and liquid water) with high resolution in time and space intervals. In this study, the predictability of precipitation occurrences and the estimation of rainfall intensity were investigated by using TBs via the MWR from 23 August 2007 to 30 June 2008 (about 10 months).

The *Rain Events* were selected by 15-min AWS rainfall data and then **RR** (Rain Record) and **NR** (No-rain Record) were created to examine the changes of TBs in 2-hour interval before raining at each frequency. The sudden increase in the variations of TB at 22-30 GHz (K-band) and 51-52 GHz in V-band was derived from the increase of the water vapor and cloud liquid water in atmosphere before raining. Based on these features, the variations of TBs at three channels of 22.2 GHz, 30.0 GHz, and 51.3 GHz were used to predict precipitation occurrences and then their performances were compared with the 3-hour operational forecasts issued at Wando observatory. Forecasts of precipitation occurrences using the MWR totally showed improved performances with smaller BIS, FAR and larger CSI than 3-hour operational forecast skills except for poor POD in less than 3.0 mm. It implies that precipitation occurrences can be predicted using the variations of TB from the MWR.

The estimation of the rainfall intensity was examined by using the close relationship between the rainfall intensity and TB of the MWR. Two methods of regression such as linear and logarithmic methods (RIE1 and RIE2) were applied to the MWR and ORG in the Haenam NCIO. A half of 10-month data were used for estimation of the regression curves and the remaining half of them were used for the forecasts of rainfall intensity and verifications. The correlation coefficients between the observed and the predicted rainfall intensity were 0.86 in linear regression (RIE1) and 0.88 in logarithmic regression (RIE2). Calculated BIS, FAR, POD, and ETS also showed noticeably improved performances for the forecasts of the rainfall intensity by the MWR. These results suggest that both RIE1 and RIE2 using the TBs of the MWR are reasonable methods for the estimation of the rainfall intensity and the performance of nonlinear regression method is better than that of linear one.

This investigation found that the MWR can be a key instrument to support the improved performance in the predictability of the precipitation occurrences and the estimation of rainfall intensity. This study also expands the flexibility of observations for improvement of the data assimilation in dynamic and thermodynamic fields together with wind profilers.

Acknowledgements. The authors are very grateful to some anonymous reviewers for providing great suggestions on this paper, which led to substantial improvement of an original manuscript. This study was carried out as a part of principal project "Development and application of technology for weather forecast" supported by the National Institute of Meteorological Research (NIMR) in the Korea Meteorological Administration (KMA).

REFERENCES

Barbaliscia, F., E. Fionda, and P. G. Masullo, 1998: Ground-based radiometric measurements of atmospheric brightness temperature and water contents in Italy. *Radio Sci.*, **33(3)**, 697−706.

Chan, P. W., and C. M. Tam, 2005: Performance and application of a multi-wavelength, ground-based microwave radiometer in rain nowcasting. *9th IOAS-AOLS of AMS.* [Available at http://radiometrics.com/chan_rain.pdf].

Chang, K.-H., S.-N. Oh, K.-D. Jeong, H.-Y. Yang, M.-J. Lee, J.-Y. Jeong, Y. Cho, H.-K. Kim, G.-M. Park, S.-S. Yum, and J.-W. Cha, 2007: Cloud Physics Observation System (CPOS) and validation of its products. *Atmosphere*, **17(1)**, 101−108. (In Korean with English abstract)

Clifford, S. F., J. C. Kaimal, R. J. Lataitis, and R. G. Strauch, 1994: Ground-based remote profiling in atmospheric studies: An overview. *Proc. IEEE*, **82**, 313−355.

Doran, J. C., S. Zhong, J. C. Liljegren, and C. Jakob, 2002: A comparison of cloud properties at a coastal and inland site at the North Slope of Alaska. *J. Geophys. Res.*, **107(D11)**, 4120, doi:10.1029/2001JD000819.

Guiraud, F. O., J. Howard, and D. C. Hogg, 1979: A dual-channel microwave radiometer designed for measurement of precipitable water and liquid. *IEEE Trans. Geosci. Electron.*, **GE-17**, 129−136.

Güldner, J., and D.Spänkuch, 1999: Results of year-round remotely sensed integrated water vapor by ground-based microwave radiometry. *J. Appl. Meteorol.*, **38**, 981−988.

_____, and _____, 2001: Remote sensing of the thermodynamic state of the atmospheric boundary layer by ground-based microwave radiometry. *J. Atmos. Oceanic Technol.*, **18**, 925−933.

Ha, J., K.-D. Park, K.-H. Chang, and H.-Y. Yang, 2007: Precision validation of GPS precipitable water vapor via comparison with MWR measurements. *Atmosphere*, **17(3)**, 291−298. (In Korean with English abstract)

Jeon, E.-H., Y.-H. Kim, K.-H. Kim, and H.-S. Lee, 2008: Operation and application guidance for the ground-based dual-band radiometer. *Atmosphere*, **18(4)**, 441−458. (In Korean with English abstract)

Kim, Y.-H. and J.-J. Baik, 2002: Maximum urban heat island intensity in Seoul. *J. Appl. Meteorl.*, **41**, 651−659.

Liu, G., C. Liu, and T. Kuo, 2001: Rainfall intensity estimation by ground-based dual-frequency microwave radiometers. *J. Appl. Meteorol.*, **40**, 1035−1041.

Meteorological Research Institute, 2003: Korea Enhanced Observing Program (KEOP) (Ⅰ−Ⅲ). METRI, 321 pp. (In Korean with English abstract)

_____, 2004: Korea Enhanced Observing Program (KEOP) (Ⅰ−Ⅳ). METRI, 362 pp. (In Korean with English abstract)

_____, 2005: Korea Enhanced Observing Program (KEOP) (Ⅰ−Ⅴ). METRI, 199 pp. (In Korean with English abstract)

_____, 2006: Korea Enhanced Observing Program (KEOP) (Ⅱ−Ⅰ). METRI, 327 pp. (In Korean with English abstract)

National Institute of Meteorological Research, 2007: Korea Enhanced Observing Program (KEOP) (Ⅱ−Ⅱ). NIMR, 343 pp. (In Korean with English abstract)

Radiometrics Corp., 2007: Profiler operator's manual. Radiometrics Corporation, 69 pp.

Solheim, F., J. R. Godwin, E. R. Westwater, Y. Han, S. J. Kiehm, K. Marsh, and R. Ware, 1998: Radiometric profiling of temperature, water vapor and cloud liquid water using various inversion methods. *Radio Sci.*, **33**, 393−404.

Yang, H.-Y., K.-H. Chang, and S.-N. Oh, 2006: Measurements of precipitable water vapor and liquid water path by dual-channel microwave radiometer during 2001-2003. *Proceedings of the Autumn Meeting of KMS*, 104−105.

Ware, R., R. Carpenter, J. Güldner, J. Liljegren, T. Nehrkorn, F. Solheim, and F. Vandenberghe, 2003: A multichannel radiometric profiler of temperature, humidity, and cloud liquid. *Radio Sci.*, **38(4)**, 8079, doi:10.1029/2002RS002856.

Wilczak, J. M., E. E. Gossard, W. D. Neff, and W. L. Eberhard, 1996: Ground-based remote sensing of the atmospheric boundary layer: 25 years of progress. *Bound.-Layer Meteor.*, **78**, 321−349.

Wilks, D. S., 1995: *Statistical Methods in the Atmospheric Sciences*. Academic Press, 467 pp.